New Journal of Physics
An Institute of Physics and Deutsche Physikalische Gesellschaft Journal

Observational limits on quantum geometry effects

Tomasz J Konopka and Seth A Major
Department of Physics, Hamilton College, Clinton, NY 13323, USA
E-mail: smajor@hamilton.edu

New Journal of Physics **4** (2002) 57.1–57.18 (http://www.njp.org/)
Received 12 March 2002, in final form 1 July 2002
Published 2 August 2002

Abstract. Using a form of modified dispersion relations derived in the context of quantum geometry, we investigate limits set by current observations on potential corrections to Lorentz invariance. We use a phenomological model in which there are separate parameters for photons, leptons and hadrons. Constraints on these parameters are derived using thresholds for the processes of photon stability, photon absorption, vacuum Čerenkov radiation, pion stability and the GZK cutoff. Although the allowed region in parameter space is tightly constrained, non-vanishing corrections to Lorentz symmetry due to quantum geometry are consistent with current astrophysical observations.

1. Introduction

The quantum description of gravitation is arguably the largest gap in our understanding of fundamental physics. In the last decade, a number of lines of research have offered new insights into the theory which will supersede quantum theory and general relativity. For instance, several approaches predict that space is fundamentally discrete. In one approach, eigenvalues of geometric observables have discrete spectra (see, e.g., [1] for a review). While it may not be surprising that the quantization of curved space yields quantized geometry, it is surprising that present day astronomical observations *already* limit the extent of quantum geometry effects [2]–[14].

These quantum geometry effects arise from the imprint of the discrete underlying space on propagating modes. Particles with ultra-high energies interact with structure on the smallest possible scales, resulting in corrections to Lorentz symmetry. Observations on the TeV scale offer an opportunity to test the extent of these quantum geometry induced Lorentz symmetry corrections.

Lorentz invariance may be the most tested symmetry in nature. Given the wealth of evidence in its support, it may seem obtuse to suggest that there may be corrections. However, there are

 © IOP Publishing Ltd and Deutsche Physikalische Gesellschaft

reasons to believe that this may not be an exact symmetry, not the least of which is the fact that any test of Lorentz invariance (necessarily at finite energy) leaves an infinite parameter space untested. Due to the non-compact nature of the Lorentz group, exact Lorentz symmetry is untestable. There are other reasons to suspect exact Lorentz invariance at all energy scales. For instance, ultraviolet divergences in quantum field theory point to new physics at high energies. Despite these suggestions, only recently has work in quantum gravity yielded concrete proposals on how the symmetry might be modified [2], [3], [15]–[18].

In this paper we explore the consequences of modified dispersion relations which are motivated by a study of semiclassical states in loop quantum gravity by Alfaro *et al* [16, 17]. We study a model in which the usual dispersion relation of special relativity, $E^2 = p^2 + m^2$, is modified by leading-order quantum geometry corrections of the form $\kappa \ell_p p^3$. By the semiclassical analysis, the parameter κ is expected to be of order unity. It determines the extent of the corrections to Lorentz symmetry while the Planck length, ℓ_p, sets the scale of the effects. Due to the sensitivity of process thresholds, the modifications of particle dispersion relations are already tested by current astronomical observations.

What is more spectacular than merely limiting the possible extent of corrections to Lorentz symmetry is the proposal [19] that this framework may be robust enough to elegantly explain three incongruities, or paradoxes, between standard model predictions and observational results:

(i) Cosmic rays are expected to interact with the cosmic microwave background (CMB), producing pions and introducing an upper limit on the observed energy of particles of cosmological origin. Known as the GZK cutoff [20, 21] this upper limit has not been observed. About twenty events at significantly higher energies have been reported [22, 23]. Modified dispersion relations can raise the GZK cutoff [5].

(ii) Ultra-high energy photons of cosmic origin are also expected to interact with infrared background radiation. According to some estimates for the background flux, photons of energy 10 TeV or more should not be seen due to background induced pair production [24]. However, higher energy events have been reported [25, 26]. Corrections to Lorentz invariance provides one explanation for this apparent paradox [6].

(iii) Observations of longitudinal development in extensive air showers of high energy hadronic particles are apparently inconsistent with predictions [27]. As proposed in [27], one possible explanation is that high energy neutral pions become stable. This may also be explained using modified dispersion relations [19].

We calculate thresholds for processes involving photons, leptons and hadrons and, with observational limits, constrain the values for the κ parameters, thereby confining the extent of quantum geometry corrections. In more detail, in the next section we summarize the results of Alfaro *et al* [16, 17]. Specifying only general properties of a semiclassical state, such as flatness above a characteristic scale L, the authors find that, in an analysis of particle propagation, photon [17] and neutrino [16] dispersion relations are modified. In section 3 we give a brief overview of threshold calculations before turning to a number of processes including: photon stability, photon non-absorption, vacuum Čerenkov radiation (VČR) for electrons and protons, proton non-absorption and pion stability. We calculate constraints from the threshold calculations to investigate whether it is possible that observed effects may be accounted for by Lorentz symmetry corrections. In 3.2 we show that asymmetric momentum partitioning, first noticed by Liberati *et al* [13], dramatically affects the constraints on the dispersion relation modifications. The results of section 3 are summarized in table 1. Finally, in section 4 we apply the constraints

together with current observations to limit the extent of potential Lorentz symmetry corrections. We summarize the constraints in the final section and in figures 2 and 3. We find that present day observations tightly constrain—but still leave open—the possibility of Lorentz symmetry corrections of this form.

Particularly close to the present work is the paper by Jacobson *et al* [13] in which many of these results were summarized. For the most part the present work agrees with this paper where the subject overlaps, although this work also includes new threshold calculations and constraints for proton VČR, the GZK threshold, and pion stability.

2. Modified dispersion relations

To determine the action of the Maxwell Hamiltonian operator on quantum geometry Alfaro *et al* specify only very general conditions for the semiclassical state. The idea is to work with a class of states which satisfy the following conditions:

(i) The state is 'peaked' on flat and continuous geometry when probed on length scales larger than a characteristic scale L, $L \gg \ell_p$.

(ii) On length scales larger than the characteristic length the state is 'peaked' on the classical Maxwell $U(1)$ connection.

(iii) The expectation values of operators are assumed to be well-defined. In addition it is assumed that the geometric corrections to the expectation values may be expanded in powers of the ratio of the physical length scales, L and ℓ_p.

States peaked on geometry and the geometric connection are the natural expectation for semiclassical or coherent states which model flat space. The work of Alfaro *et al* is a forerunner for the detailed analysis of semiclassical states. As the specification of semiclassical states becomes more precise, and work is well under way [29]–[35], we can expect to check these initial results.

Expanding the quantum Maxwell Hamiltonian on their states Alfaro *et al* find that, for massive neutrinos, the particle dispersion relations are modified with [16]

$$E_{\pm}^2 = p^2 + m^2 + (\kappa \pm \beta)\ell_p p^3 \tag{1}$$

where p is the magnitude of the 3-momentum, κ and β are of order unity and β is helicity-dependent. The result is computed for a superposition of helicity eigenstates.

For photons the authors find that the quantum geometry effects are given, to leading order in $\ell_p k$, by [17]

$$E_{\gamma}^2 = k^2 + 2\alpha k^{4+2\Upsilon}\ell_p^{2+2\Upsilon} \pm 4\beta\ell_p k^3 \tag{2}$$

where Υ parametrizes the scaling of the semiclassical state expectation value with respect to the gravitational connection. As before, the parameters α and β are of order unity with β parametrizing helicity-dependent corrections†. For the purposes of exploring the leading-order helicity-independent effects in this model of quantum geometry, we take $\Upsilon = -1/2$ and $\beta = 0$. Helicity effects have been investigated in [36] and may be treated using similar methods used in the present work.

† The specification for the class of semiclassical states is more general in [17] than in [16]. With the same specification as the photon case, the neutrino dispersion relation (1) would have the same form as (2) [28].

To place all the particles we consider on the same footing we take a phenomenological approach in which the modification to the usual dispersion is parametrized by a parameter κ_a for particle species a. Thus, the effect is simply modelled by the modified dispersion relation

$$E_a^2 = p_a^2 + m_a^2 + \kappa_a \ell_p p_a^3. \tag{3}$$

In this equation p is the magnitude of the particle 3-momentum, a quantity greater than 0†. For each particle species, the parameter κ_a is, from the semiclassical analysis, expected to be of order 1 and can take either sign. Of particular interest is to determine whether positive κ_a's are allowed for massive particles. In this case, massive particles would be able to propagate faster than the low energy speed of light, c, which has interesting repercussions for causality. Alternately, for either sign of κ_a, the particles might be able to propagate faster than high energy photons as long as $\kappa_a > \kappa_\gamma$.

In terms of bookkeeping, we use $\ell_p := \sqrt{4\pi\hbar G/c^3}$ throughout. We set the low energy speed of light to 1 ('c is 1') and $\hbar$ to 1. The scale of the model becomes $\ell_p \sim 3 \times 10^{-28}$ eV^{-1}. The effects of the correction terms become significant when the correction term is of the same magnitude as the mass term, i.e. when $p_{crit} \approx (m^2/\ell_p)^{1/3} \sim 10^{13}$, 10^{14} and 10^{15} eV for electrons, pions and protons, respectively‡.

The dispersion relation of equation (3) is not valid for all momenta. Since the class of semiclassical states identified by Alfaro *et al* only reproduces flat geometry on scales larger than L, we can only use the dispersion relation within this approximation; particles we investigate cannot have wavelengths shorter than L. Thus, the momenta are restricted by $p_a \ll 1/\ell_p$. We remain well within this restriction with $\ell_p p_a < 10^{-8}$.

We call the modification of the dispersion relations 'quantum geometry effects' since the background quantum geometry only provides the scale on which new non-linear terms enter the equations of motion. In addition the quantum geometry of the semiclassical state enjoys no reaction due to propagating modes on the geometry. It is clear that, beyond the realm of the semiclassical model, reaction of the particle on the geometry must be taken into account and we should expect new behaviour.

Throughout this discussion we assume that the momenta, energies and lengths are compared in one inertial frame. Indeed, if Lorentz symmetry is inexact then there is presumably a preferred frame (however, see, for instance, [39]–[41] for modifications of Lorentz symmetry which do not select a preferred frame). For the purposes of this phenomenological study, we work in the preferred reference frame in which the CMB radiation is isotropic.

Within the context of perturbative quantum field theory it is well known that modified dispersion relations can yield causality violations and breakdowns in perturbative quantization (see, for instance, [42]). Since we investigate particles for which the correction terms play a significant role, these issues are important. However, in the following we work in a single inertial frame and do not have the transformations between inertial frames in this new context. So we leave investigations of these issues to future work. It would be particularly interesting to

† Since equation (3) is in terms of the magnitude, the relation is invariant under time-reversal. The modification could also be viewed as a $\kappa \ell_p p^2 E$ term.

‡ Incidentally, this shows why high precision tests of Lorentz invariance such as in [37] and [38] do not offer strong limits on the κ parameters. The energies are too low. However, if the characteristic length scale of the semiclassical state were fixed at much larger scale—say, nuclear—then these high precision tests would offer limits on the analogous parameters of such a model.

precisely characterize modified dispersion relations which are consistent within the low energy perturbative framework.

3. Particle processes

On account of the modification in the dispersion relation of equation (3), quantum geometry effects are potentially observable. This is due to the sensitivity of process thresholds to the correction term for ultra-high energy particles. We outline the framework of the threshold calculations, then present the details of each of the processes in turn.

3.1. Threshold kinematics

Suppose we have the two-particle interaction $a + b \rightarrow c + d$. We assume that energy is conserved, $E_a + E_b = E_c + E_d$, and 3-momentum is conserved, $\boldsymbol{p}_a + \boldsymbol{p}_b = \boldsymbol{p}_c + \boldsymbol{p}_d$. The only unusual part is in the modified dispersion relations. Although the modified threshold calculations are a straightforward application of momentum conservation, energy conservation and the modified dispersion relations, the calculations are not without surprises. In fact, even when the outgoing particles have the same mass, it may not be energetically favourable to partition the momentum symmetrically. This asymmetry was, to our knowledge, first observed by Liberati *et al* [13].

We almost exclusively use the leading-order approximation of equation (3):

$$E \approx p + \frac{m^2}{2p} + \frac{1}{2}\kappa\ell_p p^2. \tag{4}$$

It is clear that this approximation applies for high energy particles only when $p \gg m$ so that $m \ll p \ll 1/\ell_p$.

The interaction geometry may be strongly affected by the correction term. At ultra-high momenta the correction term dominates and, if the sign of κ is negative, then the energy of the outgoing particles may be reduced by including transverse momenta. However, in the regimes we consider, using 4-momentum conservation and these modified dispersion relations it is not hard to see that the threshold interaction geometry is what one would expect: the incoming particles' momenta are antiparallel and the outgoing particles' momenta are parallel. Of course, the momenta must be sub-Planckian. We also emphasize that, in these dispersion relations, the κ parameters are of order 1. Since the framework of the semiclassical states requires that the momenta be far below the Planck scale, we employ this interaction geometry throughout the remainder of this paper.

We use the modified dispersion relation equation (4) in the conservation of energy. With energy and momentum conservation, we find the kinematic constraint

$$\frac{m_a^2}{2p_a} + \frac{1}{2}\kappa_a\ell_p p_a^2 + \frac{m_b^2}{2p_b} + \frac{1}{2}\kappa_b\ell_p p_b^2 = \frac{m_c^2}{2p_c} + \frac{1}{2}\kappa_c\ell_p p_c^2 + \frac{m_d^2}{2p_d} + \frac{1}{2}\kappa_d\ell_p p_d^2. \tag{5}$$

By momentum conservation $p_d = p_i - p_c$ with $p_i := p_a + p_b$ being the available incoming momentum. Thus the right-hand side of equation (5) may be expressed as a function of p_c only.

To locate the threshold for one of the incoming particles (typically the other momenta is known), we wish to find the minimum final energy as a function of the momentum of the outgoing

particle c. This may be accomplished by differentiating equation (5) and finding the roots. In the general two-channel case, this is given by

$$0 = -\frac{m_c^2}{2p_c^2} + \kappa_c \ell_p p_c + \frac{m_d^2}{2(p_i - p_c)^2} + \kappa_d \ell_p (p_i - p_c) \tag{6}$$

which is a quintic in p_c. With the physical root(s) in hand one can return to equation (5) to find the threshold momentum. However, in the individual processes there are better methods than attempting to directly solve this quintic. Perhaps the best way to see this is in the case of photon stability. As this case is straightforward and yet gives asymmetric partitioning we present it in its entirety.

3.2. Photon stability: $\gamma \not\to e^+ + e^-$

In special relativity photon decay is forbidden—a simple consequence of the energy and momentum conservation. However, taking quantum geometry effects into account it is energetically favourable for ultra-high energy photons to decay. Recent observations of multi-TeV photons [25, 26, 43] provide potential threshold values for the quantum geometry induced decay.

Applying the threshold framework above, we immediately see that there are considerable simplifications in equation (5). In fact, the energy–momentum constraint becomes

$$\kappa_\gamma \ell_p p_\gamma^2 = m_e^2 \left(\frac{1}{p_{e^+}} + \frac{1}{p_{e^-}} \right) + \kappa_e \ell_p (p_{e^+}^2 + p_{e^-}^2). \tag{7}$$

Before differentiating, notice that, for negative κ_γ, the electron κ parameter must also be negative. This opens up the possibility that a simple $p_\gamma/2$ partition of incoming momenta may not be energetically favourable.

This is already clear from the modified dispersion relations for negative κ_a. As the momentum of the particle increases the energy increases. However, when the momentum is near p_{crit} the energy increases less rapidly†. This curve strongly affects the nature of threshold calculations: at high momentum the slope of the energy steadily decreases so it becomes energetically favourable to partition the momentum of the outgoing particles asymmetrically. By asymmetrically partitioning momentum one can only slightly increase the energy of the high momentum particle while drastically reducing the energy of the lower momentum particle, leading to a lower total energy (for more extensive discussion see [44]).

With this observation we re-express the outgoing momenta as $p_{e^-} = p_o - \Delta$ and $p_{e^+} = p_o + \Delta$, with p_o being half the available momentum, $p_o := p_\gamma/2$. The asymmetry factor Δ can be no larger than p_o; $-p_o < \Delta < p_o$. The relation equation (7) becomes

$$2\kappa_\gamma \ell_p p_o^2 = \frac{m_e^2 p_o}{p_o^2 - \Delta^2} + \kappa_e \ell_p (p_o^2 + \Delta^2). \tag{8}$$

To find the threshold energy, or minimum energy, for this process we minimize this equation. This yields a simple quartic for Δ which has two physical roots: $\Delta_* = 0$ for the symmetric and

$$\Delta_*^2 = p_o^2 \left(1 - \sqrt{\frac{m_e^2}{-\kappa_e \ell_p p_o^3}} \right) \tag{9}$$

† At high momentum, at the limit of the semiclassical approximation, the energy reaches a maximum. Understanding what occurs at these energies requires detailed knowledge of the dynamics in addition to the semiclassical state of quantum gravity.

for the asymmetric partitioning, respectively. The second root is only real for negative κ_e. Since the momenta asymmetry is bounded by p_o there is an upper bound on κ_e for this root:

$$\kappa_e \leq -\frac{m_e^2}{\ell_p p_o^3}. \tag{10}$$

In addition, when the threshold energy is found using an asymmetric root another condition is required to ensure that all the momenta are non-negative. This condition is $\kappa_\gamma > \kappa_e$.

To find the regions of κ parameter space where the two roots impose constraints, it is worth returning to equation (8). As observed above, if κ_γ is negative then κ_e is as well. It is then energetically advantageous to asymmetrically partition the momentum, i.e. to use the non-zero root Δ_*. Thus, when both $\kappa_\gamma < 0$ and the inequality of (10) is satisfied the asymmetric configuration is applicable. With the two roots and the energy–momentum constraint, the momenta at threshold are

$$p_{\gamma_*} = \left[\frac{8m_e^2}{(2\kappa_\gamma - \kappa_e)\ell_p}\right]^{1/3} \qquad \text{for } \kappa_\gamma \geq 0$$

and (11)

$$p_{\gamma_*} = \left[\frac{-8\kappa_e m_e^2}{(\kappa_\gamma - \kappa_e)^2 \ell_p}\right]^{1/3} \qquad \text{for } \kappa_e < \kappa_\gamma < 0$$

where the two thresholds are valid in the regions identified by the inequalities.

Given a threshold value p_{γ_*} for the process, these equations give relationships between κ_e and κ_γ. Since the photon is stable if the incoming energy is less than the threshold energy, we can assign inequalities to the constraints on κ_e and κ_γ. Thus, the photon is stable at the threshold p_{γ_*} if

$$\kappa_\gamma - \frac{1}{2}\kappa_e - \frac{4m_e^2}{\ell_p p_{\gamma_*}^3} < 0 \qquad \text{for } \kappa_\gamma \geq 0$$

and (12)

$$(\kappa_\gamma - \kappa_e)^2 + \frac{8m_e^2}{\ell_p p_{\gamma_*}}\kappa_e < 0 \qquad \text{for } \kappa_e < \kappa_\gamma < 0.$$

The regions of applicability of the two constraints are inherited from the momenta thresholds. These constraints, together with the regions of applicability, determine the allowed regions in the κ parameter space.

The highest energy observed gamma ray, 50 TeV, originated from the relatively local Crab Nebula [43]. Using this energy for p_{γ_*} we plot the constraints of (12) in figure 1. The constraint inequalities ensure that the photon does not decay below this threshold. The shading represents regions in κ_e–κ_γ space which are ruled out by the constraints of (12). The smooth transition from the linear to the quadratic constraints on the κ parameters occurs when κ_γ changes sign. The resulting curve forms the upper bound on the allowed region.

There is another process which has a closely related calculation. This is the apparent paradoxical observations of TeV photons from distant sources.

3.3. Photon non-absorption: $\gamma + \gamma_{IR} \not\to e^+ + e^-$

Due to the presence of background radiation, high-energy photons are expected to be absorbed in pair creation by the far-infrared (IR) background. For photons originating from distances greater

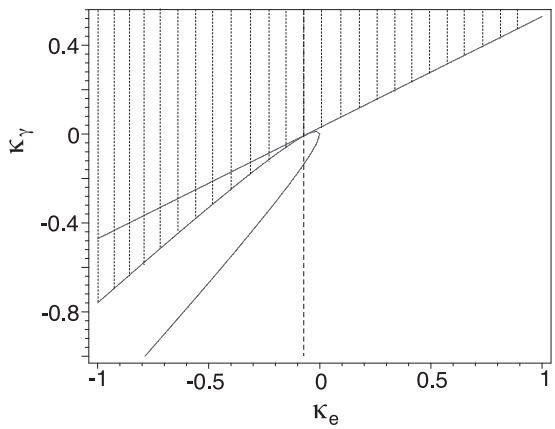

Figure 1. Using the thresholds for photon stability and a threshold value of 50 TeV, the two constraints are plotted. The two curves smoothly intersect at the transition from symmetric partitioning, the diagonal line, to asymmetric partitioning, the quadratic function in the third quadrant. The vertical broken line is the condition of equation (10). This identifies the upper branch of the asymmetric constraint as the physical solution. The region ruled out by photon stability up to 50 TeV is indicated by shading.

than $\sim$100 Mpc, the 0.025 eV background provides a cutoff in the spectrum at $\sim$10 TeV. However, recent observations of multi-TeV photons have challenged this expectation [25, 26]. Located at redshift $\sim$0.03 the active galactic nuclei Markarian 421 and Markarian 501 have produced flares with multi-TeV photons. Observations have included 17 TeV [25] and 24 Tev [26] events. It has been suggested that the apparent overabundance of high energy photons may be due to corrections to Lorentz invariance along the lines of equation (3) [10].

The process kinematics is identical with the case of photon stability of equation (8) except for the presence of the IR photon. Letting the energy of this low energy photon be ϵ, conservation of momentum for this process becomes $p_\gamma - \epsilon = p_{e^+} + p_{e^-}$ and the equation for photon absorption becomes identical to equation (8) with the substitution [13]

$$\kappa_\gamma \to \kappa'_\gamma := \kappa_\gamma + \frac{4\epsilon}{p_o^2 \ell_p}.$$

Thus, the calculation of the threshold is the same as for photon stability and the resulting κ inequalities are identical with the substitution $\kappa_\gamma \to \kappa'_\gamma$. Because of the factor of p_o in the definition of κ'_γ, it is not as straightforward to write simple expressions for p_{γ_*}. Our main interest is on the allowed regions in κ parameter space, so we are satisfied with the equations which relate κ_e and κ_γ for the allowed region. These are presented in table 1. Plots of the allowed region are similar in form to the ones for photon stability.

3.4. Pion stability: $\pi \not\to \gamma + \gamma$

Within the context of ordinary particle kinematics, the neutral pion has a lifetime of 8×10^{-17} s. As suggested by Amelino-Camelia [19], the modified dispersion relations can have the effect of making ultra-high energy neutral pions stable. This may explain some inconsistencies between observed and expected patterns in cosmic ray showers.

Table 1. Summary of constraints and their regions of applicability.

Process type	Constraint	Applicability
	Photon stability ($\gamma \not\to e^- + e^+$)	
Symmetric momenta	$\kappa_\gamma < \frac{1}{2}\kappa_e + \frac{4m_e^2}{\ell_p p_{\gamma_*}^3}$	$\kappa_\gamma \geq 0$
Asymmetric momenta	$(\kappa_\gamma - \kappa_e)^2 + \frac{8m_e^2\kappa_e}{p_{\gamma_*}^3 \ell_p} < 0$	$\kappa_e < \kappa_\gamma < 0$
	Photon non-absorption ($\gamma + \gamma_{IR} \not\to e^- + e^+$)	
Symmetric momenta	$2\kappa_\gamma + \frac{8\epsilon}{\ell_p p_{\gamma_*}^2} - \kappa_e - \frac{8m_e^2}{\ell_p p_{\gamma_*}^3} < 0$	$\kappa_\gamma > -\frac{4\epsilon}{\ell_p p_{\gamma_*}}$
Asymmetric momenta	$\left(\kappa_\gamma + \frac{4\epsilon}{\ell_p p_{\gamma_*}^2} - \kappa_e\right)^2 + \frac{8m_e^2\kappa_e}{p_{\gamma_*}^3 \ell_p} < 0$	$\kappa_\gamma < -\frac{4\epsilon}{\ell_p p_{\gamma_*}}$
	Pion stability ($\pi \not\to \gamma + \gamma$)	
Symmetric momenta	$\kappa_\gamma < 2\kappa_\pi + \frac{2m_\pi^2}{\ell_p p_{\pi_*}^3}$	$\kappa_\gamma > 2\kappa_\pi$ and $\kappa_\gamma > 0$
Asymmetric momenta	$\kappa_\gamma < \kappa_\pi + \frac{m_\pi^2}{\ell_p p_{\pi_*}^3}$	$\kappa_\gamma > \kappa_\pi$ and $\kappa_\gamma < 0$
	Proton stability ($p + \epsilon \not\to p + \pi$)	
Numerical result	$\kappa_p < -8 \times 10^{-16}$	
	Vacuum Čerenkov radiation ($a \not\to a + \gamma$)	
Type I: zero-energy photon	$\kappa_a < \frac{m_a^2}{2\ell_p p_{a_*}^3}$	$\kappa_\gamma > 0$ or $\kappa_e > 0$
Type II: finite-energy photon	$\kappa_\gamma > \kappa_a - \frac{m_a^2}{2\ell_p p_{a_*}^3}$	$\kappa_\gamma < 0$
Energy conservation	$(\kappa_a - \kappa_\gamma)^2 + \frac{4m_a^2}{\ell_p p_{a_*}^3}(\kappa_a + \kappa_\gamma) < 0$	$\kappa_\gamma < 0, \kappa_\gamma < \kappa_a, \kappa_\gamma < -3\kappa_a$

Normally the pion decays because the rest mass can be converted into energy in the form of photons. With the modified dispersion relations, it is possible that, above a threshold energy, it is no longer kinematically possible for the pion to decay.

The threshold calculation is similar to photon stability. Proceeding as before we asymmetrically partition the available momentum for the two photons, $p_o - \Delta$ and $p_o + \Delta$. The resulting energy–momentum constraint is

$$\frac{m_\pi^2}{2p_o} + 4\kappa_\pi \ell_p p_o^2 = 2\kappa_\gamma \ell_p (p_o^2 + \Delta^2). \tag{13}$$

As is clear from this equation the analysis splits into two cases, depending on the sign of κ_γ. For $\kappa_\gamma > 0$ the minimization requires symmetric partitioning: $\Delta_* = 0$. Solving equation (13) for the threshold momentum we have

$$p_{\pi_*} = \left[\frac{2m_\pi^2}{(\kappa_\gamma - 2\kappa_\pi)\ell_p}\right]^{1/3} \qquad \text{for } \kappa_\gamma > 0 \text{ and } \kappa_\gamma > 2\kappa_\pi. \tag{14}$$

The last inequality ensures that the momentum is positive.

In the second case, $\kappa_\gamma < 0$, the symmetric partitioning is, in fact, the worst choice we could make. Equal photon momenta is the maximum of the outgoing energy. The local minimum for the energy of the outgoing photons is at the maximum possible asymmetry, $\Delta_* = p_o = p_\pi/2$, corresponding to the threshold emission of a zero-momentum photon. From equation (13), the threshold momentum for this process is bounded from below:

$$p_{\pi_*} > \left[\frac{m_\pi^2}{(\kappa_\gamma - \kappa_\pi)\ell_p}\right]^{1/3} \qquad \text{for } \kappa_\gamma < 0 \text{ and } \kappa_\gamma > \kappa_\pi. \tag{15}$$

The first inequality for κ_γ ensures that the energy remains positive while the last ensures that the threshold momentum is positive.

In an identical manner to the previous calculations, equations (14) and (15) yield inequalities among κ_π and κ_γ. These are summarized in table 1.

3.5. Vacuum Čerenkov radiation: $a \to a + \gamma$

Čerenkov radiation is observed when a charged particle enters a medium with a speed greater than the phase velocity of electromagnetic waves in the medium. VČR in which empty flat space constitutes the medium is normally forbidden by ordinary threshold kinematics. However, Coleman and Glashow suggested that, within the context of a variable-speed-of-light theory, VČR could be induced when a charged particle's speed exceeds the local speed of light [4] (see also [11]). VČR may also be kinematically allowed by the modified dispersion relations. This is clear even from a glance at a charged particle's speed:

$$v_a = \frac{\partial E_a}{\partial p_a} = 1 - \frac{m_a^2}{2p_a^2} + \kappa_a \ell_p p_a \tag{16}$$

where a is the charged particle.

Since both charged particles and photons have the same functional form of the dispersion relations, there are four possible cases to investigate. These depend on the signs of κ_γ and κ_a:

(i) For $\kappa_\gamma > 0$ and $\kappa_a < 0$ no radiation occurs.

(ii) For $\kappa_\gamma > 0$ and $\kappa_a > 0$ VČR may occur when the charged particle's speed exceeds 1, the low energy speed of light. We call this Type I VČR.

(iii) For $\kappa_\gamma < \kappa_a$ VČR occurs either when the charged particle's speed exceeds the low energy speed of light or when it exceeds the speed of the ultra-high energy photon.

We call this last case Type II VČR. These cases show that VČR could occur in the first, fourth and part of the third quadrants.

We present the threshold calculation first for a charged particle a. In section 4 we use these results for electrons and protons. The threshold calculations can be found using the methods employed above or, equivalently, using the Čerenkov condition $v_a > v_\gamma$. Using the latter method we find that, for high energy charged particles, the condition for Type I VČR is

$$p_{a_*} = \left[\frac{m_a^2}{2\ell_p\kappa_a}\right]^{1/3} \qquad \text{for } \kappa_a > 0. \tag{17}$$

This condition corresponds to the momentum at which the particle's speed exceeds 1, the low energy speed of light. This process of photon emission begins with long wavelength photons. For this type I radiation the spectrum extends from zero energy up to $p_{\gamma_{max}} = p_{a_*}$.

When $\kappa_\gamma < \kappa_a$, however, the emission process starts with finite energy photons. For high energy particles and photons—what we call type II VČR—the Čerenkov condition yields

$$p_{a_*} = \left[\frac{m_a^2}{2(\kappa_a - \kappa_\gamma)\ell_p}\right]^{1/3} \qquad \text{for } \kappa_a > \kappa_\gamma. \tag{18}$$

This may also be derived using the methods of section 3.2. The observational constraints may be derived from this threshold.

When using the velocity relation, one must also ensure that energy is conserved. We study the case in which both outgoing particles have high momenta. In the leading order approximation of equation (4), the energy–momentum constraint takes on the familiar form of the threshold calculations:

$$\frac{m_a^2}{p_a} + \kappa_a\ell_p p_a^2 = \frac{m_a^2}{(p_a - p_\gamma)} + \kappa_a\ell_p(p_a - p_\gamma)^2 + \kappa_\gamma\ell_p p_\gamma^2.$$

After some simplification, this gives a quadratic for p_γ

$$p_\gamma^2 - \frac{(3\kappa_a + \kappa_\gamma)p_a}{(\kappa_a + \kappa_\gamma)}p_\gamma - \frac{m_a^2 - 2\kappa_a\ell_p p_a^3}{(\kappa_a + \kappa_\gamma)\ell_p p_a} = 0. \tag{19}$$

The requirements that the physical root of this equation, p_{γ_*}, be real and positive produce the threshold value

$$p_{a_*} = \left[\frac{-4m_a^2(\kappa_a + \kappa_\gamma)}{(\kappa_a - \kappa_\gamma)^2\ell_p}\right]^{1/3} \qquad \text{for } \kappa_\gamma < -3\kappa_e < 0. \tag{20}$$

The last inequality arises from the positivity of the maximum energy outgoing photon:

$$p_{\gamma_*} = \frac{(3\kappa_a + \kappa_\gamma)}{2(\kappa_a + \kappa_\gamma)}p_{a_*}. \tag{21}$$

The two types of VČR have distinct spectra. For type I, the emission of photons starts with very low energy photons and extends up to the particle's energy $p_{\gamma_{max}} = p_a$. For type II VČR, the spectrum forms a band which begins at the finite energy corresponding to the condition

$v_a(p) = c_\gamma(p)$ and extends up to the particle's energy p_a. The half-angles of the Čerenkov cone apertures also differ for the two types of radiation. The angle may be simply computed from equation (16). For type II,

$$\theta_C \approx \left[\frac{m_a^2}{p_a^2}(1 - \kappa_\gamma \ell_p p_\gamma) - 2\kappa_a \ell_p p_a\right]^{1/2}. \tag{22}$$

The angle for type I is found by setting $\kappa_\gamma = 0$ in the above equation.

Using observations of high energy electrons and protons, we can establish limits on the possible values of κ_e and κ_p. This is done in the final section.

3.6. Proton non-absorption: $p + \gamma \not\rightarrow p + \pi^0$

Shortly after the CMB was discovered, Greisen [20] and Zatsepin and Kuzmin [21] predicted that the cosmic ray spectrum should have a cutoff. They found that cosmic ray constituents, including protons and some heavier nuclei arriving from cosmological distances, would lose energy through interactions with the CMB photons. The dominant process, photopion production, provides an effective energy cutoff for high energy protons from cosmological sources. In fact the spectrum was believed to be bounded from above by 5×10^{19} eV. However, the observed spectrum extends well above this cutoff to 3×10^{20} eV. While the number of events with energies above the GZK cutoff is not large ($\sim$20), the locations on the sky are not inconsistent with the hypothesis that the sources are isotropic. If these events are indeed particles originating from cosmological distances, then the GZK cutoff must be modified. As observed in [5], the modified dispersion relations considered here can raise the GZK cutoff.

The method for computing the threshold energy for photopion production is similar to the above process but the details make the problem more complex. The different masses of the pion and proton mean that much of the simplifications used above do not work. This returns us to the general two-channel case and the resulting quintic for the momentum p_c. In addition, when κ_p is negative, large asymmetries are favoured. In fact, the threshold process produces a low momentum pion, which means that we must use the dispersion relations of equation (3) instead of the leading-order approximation. Hence the constraint on κ_p was found numerically.

Using threshold values in the range 1×10^{19}–8×10^{20} eV we performed a search for the value of κ_p which separated the parameter space into a region in which the high energy proton would be stable and a region where it would be unstable. The selection criteria were simply that $E_p + \epsilon > E'_p + E_\pi$, where the energies are expressed using the modified dispersion relations of equation (3), and ϵ is the energy of the CMB photon, 7×10^{-4} eV. Conservation of 3-momentum was also required. Since the κ parameters for both pion and proton are identical, the procedure produced a constraint on κ_p as a function of proton threshold energy.

This function has the familiar shape of the effective potential of a particle in a central potential. At energies below the GZK cutoff κ_p is positive, effectively lowering the threshold. At the GZK cutoff κ_p passes through zero. However, the dependence of κ_p on the threshold energy is not a monotonically decreasing function. To see this, note that, since the magnitude of the proton correction term is larger than the magnitude of the correction terms of the products, at energies above the GZK cutoff κ_p must be negative. At significantly higher energies κ_p approaches zero from below (as may also be seen with energy–momentum conservation in the leading-order approximation). The resulting function has a minimum of -7.9×10^{-16} at 1.6×10^{20} eV. Thus, measurements of higher energy cosmic rays will not restrict the parameter further. These results are discussed further in the next section.

4. Limits on κ parameters

With all the above processes, one can derive limits on the modifications to the dispersion relations. The threshold constraints of section 3 determine the allowed regions in the κ_e–κ_γ and κ_p–κ_γ parameter spaces. These constraints are summarized in table 1. With the threshold energies in hand one can plot the constraints and determine the allowed regions. But before discussing these plots, we summarize the observational data which provide threshold values for each of the processes.

We already discussed in section 3.2 the observation which we use for photon stability (the 50 TeV event from the Crab Nebula). We now turn to photon non-absorption by the far-infrared background.

The unexpected transparency of the universe for high energy photons may be due to Lorentz symmetry corrections (see, however, [45]). Although direct measurements from two instruments on board COBE and detailed calculations have been completed, the IR flux is not well determined [46]. This is largely due to, on the observational side, the flux of IR radiation produced by interplanetary dust and, on the calculational side, uncertainties in the galactic-evolution models. Given the uncertainties in the IR flux, we only plot an example case. The photon non-absorption constraint has a complex dependence on energy. Nonetheless, in the relevant region the threshold energy which allows for the maximum increase in transparency due to suppressed pair creation induced by background 0.025 eV IR photons is 15 TeV. In the summary plots we use this energy as a representative case. If the unexpected transparency is due to Lorentz symmetry corrections then this constraint is the lower boundary on the allowed region.

At shorter wavelengths the spectrum is much better established. In fact, with no modifications the universe becomes highly opaque to photons above $\sim$100 TeV from the interactions with the 2.7 K cosmic background radiation [46]. Observations of photons above this 'hard limit' would necessitate more serious consideration of photon non-absorption due to modifications to Lorentz symmetry.

As shown in section 3.4 modified dispersion relations can make the pion stable (see also [4, 19]). Recently Antonov *et al* [27] reported on a test of Lorentz invariance using longitudinal development of extensive cosmic air showers. They found that simulated air showers produced a better fit to the observed depth of the highest energy air shower [22] if the pion became stable at high energies. This stability could be achieved if pions are stable above $p_{\pi_*} \sim 10^{18}$ eV. We use this threshold value in the κ_p–κ_γ plot. This becomes a very restrictive limit.

VČR provides a strong restriction 'from the bottom' in κ_a–κ_γ parameter space. We consider limits on the allowed region in the parameter space for both electrons and protons. The limit for electrons comes from observations of a supernova remnant. The best fit for the x-ray spectrum from the supernova remnant SN 1006 arises from assuming that the radiation is synchrotron radiation from electrons with energies up to $\sim$100 TeV [47, 48]. The highest energy primary cosmic rays are believed to be protons [27]. As we see next the cosmic ray spectrum reaches 3×10^{20} eV. We use this limit for VČR for protons.

Finally, cosmic rays above the GZK cutoff are observed. This cutoff may be raised by modified dispersion relations. Using the highest observed cosmic ray, 3×10^{20} eV for the threshold, we would obtain the constraint $\kappa_p < -5.6 \times 10^{-16}$. There are two interesting features to this result. First, there is a minimum at 1.6×10^{20} eV in the κ_p energy curve discussed in

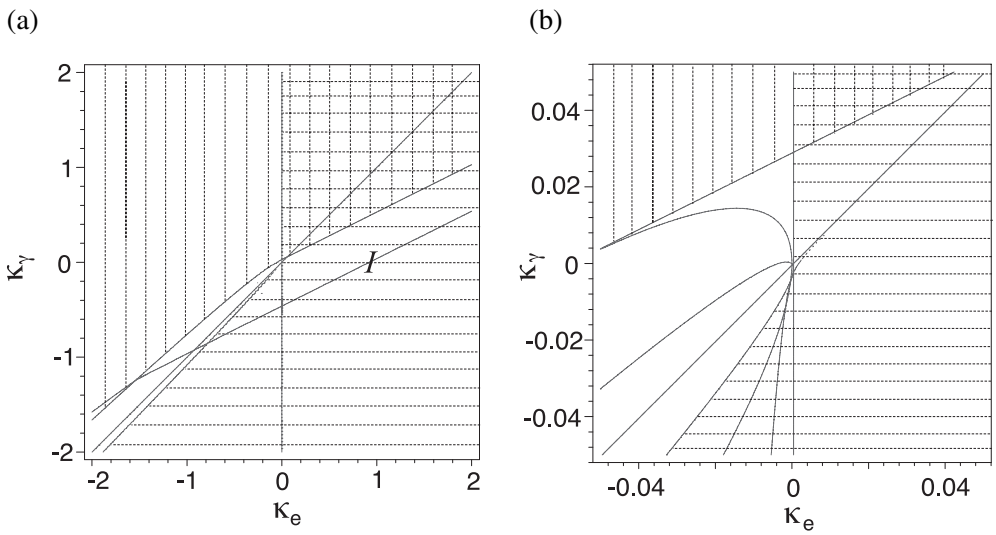

Figure 2. Plots of the allowed regions in κ_γ–κ_e parameter space. The unshaded portion shows the region in which corrections to Lorentz invariance are consistent with current observational limits. In (a) limits from photon stability, VČR and photon non-absorption are shown. The vertical shading corresponds to the photon stability constraint while the horizontal shading corresponds to VČR. The constraint labelled I arises from assuming that high energy photons are not absorbed in pair creation. If so, this provides a lower limit on the allowed region. In (b) the same constraints are shown in a region around the origin. The shading is the same as in (a).

section 3.6. To prevent a gap in the cosmic ray spectrum between 1.1×10^{20} and 3×10^{20} eV we use the value of κ_p at the minimum, -8×10^{-16}. Second, even when one accounts for the uncertainties reported in [22] the constraint is not consistent with $\kappa_p = 0$. Attributing the raising of the GZK threshold modifications of the dispersion relations restricts the hadronic parameter to negative values and effectively rules out exact Lorentz invariance.

In figures 2 and 3 we identify the allowed regions of κ_e–κ_γ and κ_p–κ_γ parameter space. We include all the above processes, including the more speculative processes of photon non-absorption, proton non-absorption and pion stability. This allows us to check whether a consistent set of parameters exist which simultaneous explain the three paradoxes mentioned in the introduction and are consistent with current observations.

In the electron–photon plot of figure 2 we include constraints from photon stability, VČR and photon non-absorption. The allowed region is a tightly constrained area mostly lying in the third quadrant and containing the origin. Thus, based on these processes it appears that quantum geometry effects reduce the energy (and speed) of particles at high momentum. As figure 2(b) reveals, however, there is a region in which positive values of the parameters are allowed. The allowed region contains the origin and a tiny sliver of positive κ_e corresponding to superluminal electrons ($\kappa_e < 4.5 \times 10^{-4}$). The κ_γ parameter is not as tightly confined around the origin and is less than ~ 0.03.

In the hadron–photon plot of figure 3 the limits are obtained from the processes of pion stability, proton non-absorption and VČR. The quadratic VČR constraints do not show up on this

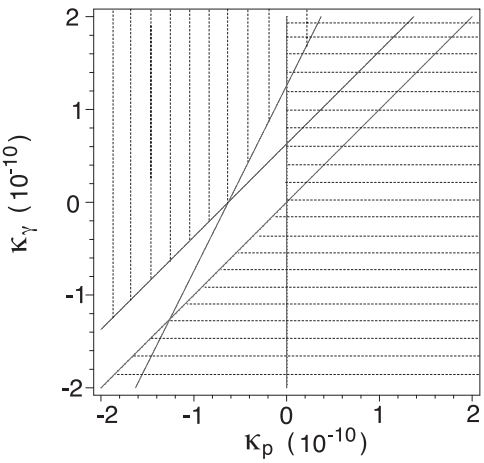

Figure 3. The plot of the allowed region in the κ_γ–κ_p space. Constraints arising from pion stability, proton non-absorption and VČR are shown. The vertical shading is due to the pion stability constraint while the horizontal shading comes from VČR. The constraints due to proton non-absorption and VČR appear to be a single vertical line.

scale due to the high upper limit on proton energy, 3×10^{20} eV. In this plot the allowed region is a exceedingly narrow band, again mostly in the third quadrant; the scale is of the order of 10^{-10}. There is a small region of positive values of the parameters allowed. The band of allowed values is constrained by the pion stability from above and VČR from below.

If these two constraints are borne out by further observations, different modifications of Lorentz invariance of this form for hadronic and massless particles would be effectively ruled out. It is also interesting that the case $\kappa_p = \kappa_\gamma$ lies nearly on the boundary of the allowed region. The difference of this relation and the VČR constraint is $\sim 10^{-15}$.

We also note that the allowed region does *not* contain $\kappa_p = 0$, the Lorentz symmetric case. This is due to the raising of the GZK threshold. It is likely that the GZK threshold may be explained by other means. Nonetheless, if the GZK cutoff is raised by corrections of this form, then current observations rule out exact Lorentz symmetry. So if we take the three conditions of pion stability, proton non-absorption and VČR seriously, then the Lorentz symmetry is broken and the parameters are extremely finely tuned to each other. From the plot and the constraints on κ from the semiclassical analysis, we conclude that $\kappa_p = \kappa_\gamma \neq 0$.

Finally, it is also clear that nearly all the positive κ space is ruled out. In particular, the results for massive particles effectively rule out 'faster than light' behaviour. One reason why this is significant is that it satisfies the classical notion of causality, thereby satisfying one of the requirements for consistency in perturbative quantum field theory.

It is important to keep in mind that these are preliminary results. Our strategy is to combine all processes to see whether the results are consistent. But it is clear that these constraints are not equally precise. For instance, the VČR constraints are tentative. The limits for electrons are derived from indirect measurements of synchrotron radiation around a single supernova remnant. We need more data on high energy electrons and cosmic rays before these processes can truly rule out regions of the parameter space.

Our VČR limit for hadrons could also be called 'soft.' We assume that the highest energy cosmic ray event was due to a proton. As new cosmic ray data becomes available we will be able to better judge the validity of this assumption. Once the Pierre Auger project [49] is running we should have a much better idea of the value of the threshold. Aside from data from more ultra-high energy events, this detector should also determine the mass composition of the primary cosmic rays. This is absolutely critical for the study of Lorentz symmetry modifications.

Much better estimates of the far-infrared background are needed before we can establish the lower limit of the allowed region in κ_e–κ_γ parameter space. Without this bound we cannot confine the parameters to a finite area. In [13] the uncertainty is the background is handled in a different way. Assuming that the actual threshold lies between 10 and 20 TeV they confine the allowed area to a finite size.

The pion stability constraint will also be improved with new cosmic ray data. The results of [27] compare simulated showers with the single, highest energy cosmic ray event [22]. It will be very interesting to see whether the onset of pion stability is observed in other ultra-high energy showers.

The only constraint which could be considered a hard limit comes from photon stability. This sharply restricts the possible superluminal behaviour of ultra-high energy photons. As higher energy gammas are observed from local sources, this constraint will 'push down' on the allowed region.

5. Conclusions

Beginning with a form of modified dispersion relations, we use exact energy–momentum conservation to derive thresholds for particle processes. The dispersion relations we consider are motivated by a class of semiclassical states of loop quantum gravity which are classical and flat above a characteristic length scale [16, 17]. We work in a model in which there are separate parameters for modifications of the dispersion relations for photons, leptons and hadrons. The process thresholds provide a sensitive test of the quantum geometry effects. In some cases, such as photon decay and VČR, normally forbidden processes are activated at high energy. In other cases, such as pion decay, processes are suppressed.

Current TeV scale observations offer severe restrictions on the nature of these effects. There exist allowed regions in both parameter spaces consistent with all of the above processes. The results are summarized in figures 2 and 3 and in the last section. In particular, including all of the processes the analysis shows that the hadronic parameter is effectively equal to the photon parameter and both of these are non-zero. Further the lepton parameter is confined to a band in the third quadrant as shown in figure 2.

Acknowledgments

We thank members of the Hamilton College Department of Physics, the Perimeter Institute, Hugo Morales-Técotl and David Mattingly for helpful discussions during this work. T K was supported, in part, by the Ralph E Hansmann Science Students Support Fund of Hamilton College.

References

[1] Rovelli C 1998 Loop quantum gravity *Living Reviews in Relativity* http://www.livingreviews.org/Articles/Volume1/1998-1rovelli
Gaul M and Rovelli C 2000 *Loop Quantum Gravity and the Meaning of Diffeomorphism Invariance (Lecture Notes in Physics* vol 541) pp 277–324 (*Preprint* gr-qc/9910079)
[2] Kostelecky V A and Samuel S 1989 *Phys. Rev.* D **39** 683
[3] Amelino-Camilia G *et al* 1998 *Nature* **393** 763
[4] Coleman S and Glashow S L 1999 *Phys. Rev.* D **59** 116008
[5] Kifune T 1999 *Astrophys. J.* **518** L21
[6] Kluzniak W 1999 *Astropart. Phys.* **11** 117
[7] Bertolami O and Carvalho C S 2000 *Phys. Rev.* D **61** 103002
[8] Ellis J, Mavromatos N E and Nanopoulos D V 1999 Probing models of quantum space-time foam *Preprint* gr-qc/9909085
[9] Aloisio R *et al* 2000 *Phys. Rev.* D **62** 053010
[10] Amelino-Camilia G and Piran T 2001 *Phys. Rev.* D **64** 036005
[11] Stecker F W and Glashow S L 2001 *Astropart. Phys.* **16** 97
[12] Ellis J, Mavromatos N E and Nanopoulos D V 2001 Space-time foam effects on particle interactions and the GZK cutoff *Phys. Rev.* D **63** 124025 (*Preprint* hep-th/0012216)
[13] Jacobson T, Liberati S and Mattingly D 2001 TeV Astrophysics constraints on Planck scale Lorentz violation *Preprint* hep-ph/0112207
See also Jacobson T, Liberati S and Mattingly D 2001 High energy constraints on Lorentz symmetry violations *Preprint* hep-ph/0110094
[14] Alfaro J and Palma G 2002 *Phys. Rev.* D **65** 103516
[15] Gambini R and Pullin J 1999 *Phys. Rev.* D **59** 124021
[16] Alfaro J, Morales-Técotl H A, Urrutia L F 1999 Quantum gravity corrections to neutrino propagation *Phys. Rev. Lett.* **84** 2318 (*Preprint* gr-qc/9909079)
[17] Alfaro J, Morales-Técotl H A and Urrutia L F 2002 Loop quantum gravity and light propagation *Phys. Rev.* D **65** 103509 (*Preprint* hep-th/0108061)
[18] Bruno N R, Amelino-Camelia G and Kowalski-Glikman J 2001 *Phys. Lett.* B **522** 133
[19] Amelino-Camilia G 2001 Space-time quantum solves three experimental paradoxes *Preprint* gr-qc/0107086
[20] Greisen K 1966 *Phys. Rev. Lett.* **16** 748
[21] Zatsepin G T and Kuzmin V A 1966 *JETP Lett.* **41** 78
[22] Bird D J *et al* 1994 *Astrophys. J.* **424** 491
[23] Takeda M *et al* 1998 *Phys. Rev. Lett.* **81** 1163
[24] Protheroe R J and Meyer H 2000 *Phys. Lett.* B **493** 1–6
[25] Krennrich F *et al* 2001 *Preprint* astro-ph/0107113
[26] Aharonian F A 1999 *Astron. Astrophys.* **349** 11A
[27] Antonov E E *et al* 2001 *JETP Lett.* **73** 446
[28] Morales-Técotl H A 2002 Private communication
[29] Varadarajan M and Zapata J 2000 A proposal for analyzing the classical limit of kinematic loop gravity *Class. Quantum Grav.* **17** 4085–109
[30] Thiemann T 2001 *Class. Quantum Grav.* **18** 2025
[31] Thiemann T and Winkler O 2001 *Class. Quantum Grav.* **18** 2561–636
Thiemann T and Winkler O 2001 *Class. Quantum Grav.* **18** 4629–82
Thiemann T and Winkler O 2001 *Class. Quantum Grav.* **18** 4997–5054
[32] Sahlmann H, Thiemann T and Winkler O 2001 *Nucl. Phys.* B **606** 401–40
[33] Corichi A and Reyes J 2001 A Gaussian weave for kinematical loop quantum gravity *Int. J. Mod. Phys.* D **10** 325–38

[34] Varadarajan M 2001 Photons from quantized electric flux representations *Phys. Rev.* D **64** 104003
[35] Ashtekar A and Lewandowski J 2001 Relation between polymer and Fock excitations *Class. Quant. Grav.* **18** L117–28
[36] Gleiser R and Kozameh C 2001 Astrophysical limits on quantum gravity motivated birefringence *Phys. Rev.* D **64** 083007
[37] Bear *et al* 2000 *Phys. Rev. Lett.* **85** 5038
[38] Berglund *et al* 1995 *Phys. Rev. Lett.* **75** 1879
[39] Kowalski-Glikman J and Nowak S 2002 *Preprint* hep-th/0203040
[40] Amelino-Camilia G 2001 *Phys. Lett.* B **510** 255–63
Amelino-Camilia G 2002 *Int. J. Mod. Phys.* D **11** 35–60
[41] Maguejo J and Smolin L 2001 Lorentz invariance with an invariant energy scale *Preprint* hep-th/0112090
[42] Kostelecky V and Lehnert R 2001 Stability, causality, and Lorentz and CPT violation *Phys. Rev.* D **63** 065008
[43] Tanimori T *et al* 1998 *Astrophys. J.* **492** L33
[44] Konopka T 2001 Quantum gravity effects on ultra high energy particles *BA Thesis* Hamilton College
[45] de Jager O C and Stecker F W 2002 *Astrophys. J.* **566** 738 (*Preprint* astro-ph/0107103)
[46] Berezinsky V 2001 Puzzles in astrophysics in the past and present *Preprint* astro-ph/0107306
[47] Reynolds S 1996 Synchrotron models for x-rays from the supernova remnant SN 1006 *Astrophys. J.* **459** L13
[48] Koyama K *et al* 1995 *Nature* **378** 255
[49] See The Pierre Auger Project www.auger.org